Author Manuscript

Author Manuscript

Author Manuscript

Author Manuscript

HHS Public Access

Author manuscript

J Mater Chem B. Author manuscript; available in PMC 2020 December 14.

Published in final edited form as:

J Mater Chem B. 2019 December 14; 7(46): 7406–7414. doi:10.1039/c9tb00630c.

PEGylated Reduced-Graphene Oxide Hybridized with Fe_3O_4 Nanoparticles for Cancer Photothermal-Immunotherapy

Lu Wang[‡,a,b], **Meng Wang**[‡,b,c], **Benqing Zhou**[b,c], **Feifan Zhou**[c,b], **Cynthia Murray**[b], **Rheal A. Towner**[d], **Nataliya Smith**[d], **Debra Saunders**[d], **Gang Xie**[a], **Wei R. Chen**[b,*]

[a]Key Laboratory of Synthetic and Natural Functional Molecule Chemistry of Ministry of Education, College of Chemistry & Materials Science, Northwest University, Xi'an, Shaanxi 710069, P. R. China

[b]Biophotonics Research Laboratory, Center for Interdisciplinary Biomedical Education and Research, College of Mathematics and Science, University of Central Oklahoma, Edmond, Oklahoma 73034, United States

[c]Key Laboratory of Optoelectronic Devices and Systems of Ministry of Education and Guangdong Province, College of Optoelectronic Engineering, Shenzhen University, Shenzhen, Guangdong 518060, P. R. China

[d]Advanced Magnetic Resonance Center, Oklahoma Medical Research Foundation, Oklahoma City, Oklahoma 73104, United States

Abstract

Photoimmunotherapy has attracted much attention recently for the treatment of metastatic tumors. The development of smart nanocomposites for imaging-guided therapies are needed to improve the efficacy of cancer treatment. Herein, a PEGylated nanocomposite was developed for photothermal-immunotherapy. In particular, this nanocomposite was formulated by hybridizing Fe_3O_4 nanoparticles (FNPs) with reduced-graphene oxide (rGO) through electrostatic interaction, modified by PEG-NH_2 on the surface of FNPs/rGO. The FNPs/rGO-PEG nanocomposites are excellent agents for photothermal therapy (PTT) under irradiation by an 805-nm laser. This nanocomposite could promote the activity of the host antitumor immune response efficiently because of the reduction of tumor-associated macrophages by the incorporation of FNPs. In our experiments, we observed FNPs/rGO-PEG based PTT induced immunogenic cell death accompanied by release of danger-associated molecular patterns. We also found that FNPs/rGO-PEG + laser irradiation of animal tumors could activate dendritic cells (DCs) in tumor draining lymph nodes. *In vivo* antitumor studies revealed that FNPs/rGO-PEG nanocomposites, when combined with laser irradiation, could result in desirable photothermal effects and destroy primary tumors. Moreover, intratumoral injection of FNPs/rGO-PEG nanocomposites into 4T1 orthotopic mouse breast tumors, in combination with near-infrared laser irradiation, significantly increased

*Corresponding Author: Wei R. Chen (wchen@uco.edu).

‡Lu Wang and Meng Wang contributed equally to this work.

†Electronic Supplementary Information (ESI) available: [details of any supplementary information available should be included here]. See DOI: 10.1039/x0xx00000x

Conflicts of interest

There are no conflicts to declare.

Author Manuscript Author Manuscript Author Manuscript Author Manuscript

the median survival time of tumor-bearing animals. FNPs/rGO-PEG nanocomposites also could be used for magnetic resonance imaging, which may lead to a MRI-guided photothermal-immunotherapy for metastatic cancers. This study could lead to a cancer treatment strategy that combines PTT with immunotherapies using FNPs/rGO-PEG nanocomposites.

Graphical Abstract

A novel nanocomposite was designed by hybridizing Fe_3O_4 nanoparticles with reduced-graphene oxide for imaging-guided photothermal-immunotherapy. This nanocomposite is an excellent agent for photothermal therapy and could facilitate a tumor-specific immune response to inhibit tumor metastasis.

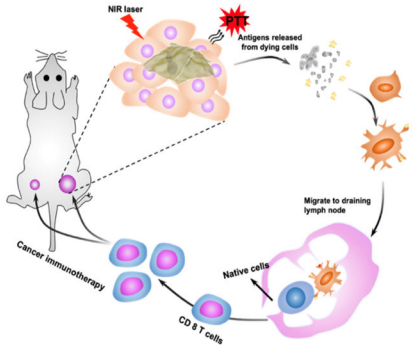

Introduction

Tumor metastasis has been the main challenge in current cancer treatment and also leads to 90% of cancer-caused deaths.[1,2,3] Conventional cancer therapies, such as chemotherapy, radiotherapy, and surgery can be effective in eliminating primary tumors, though often useless for systemic inhibition and/or eradication of metastasis.[4] Recently, immunotherapies have achieved promising results against metastatic cancers, such as cytokine therapy,[5] immune checkpoint blockade therapy,[6] and adoptive cell therapy.[7] However, traditional immunotherapies are often expensive and can have toxic side effects.[8,9] To achieve superior therapeutic effects against metastatic breast cancer, multimodal therapies combined with immunotherapies have recently been developed, such as chemo-immunotherapies,[10–13] radio-immunotherapies,[14,15] and photothermal therapy (PTT) - immunotherapies.[17] As an effective therapy for cancer, the combination of PTT and immunotherapy has shown great promise.[6, 18–21] PTT ablates tumor cells with heat generated from the absorbed optical energy by light-absorbing agents that accumulate in the tumors.[22,23] Furthermore, the process of PTT treatment also produces tumor-associated antigens by causing immunogenic cell death (ICD), which can lead to antitumor immunity in the body. However, low penetration depth and limited immune stimulation are still the major obstacles for PTT. Therefore, it's important to develop a new treatment strategy which combines with PTT and immunotherapy.

Recently, it has been discovered that some inorganic nanoparticles themselves can act as immunostimulants to activate the body's immune system, such as carbon nanotubes, graphene oxide, and silicon quantum dots.[24–28] Specifically, PEGylated reduced-graphene

Author Manuscript Author Manuscript Author Manuscript Author Manuscript

oxide (rGO) can activate macrophages by triggering a potent release of cytokines; additionally, it is an excellent photothermal agent and it has been used in PTT. Using PEGylated-rGO in photo-immunotherapy is expected to improve efficacy in treating animal tumors.[29] Recently, Fe_3O_4 nanoparticles (FNPs) have been used in cancer immunotherapy because they can regulate the microenvironment of tumors and reduce the body's immune suppression.[30–33] Due to their biocompatibility, FNPs have been considered as a promising candidate for MRI contrast agent for cancer therapy with hyperthermia.[34, 35] Therefore, the use of FNPs in combination with rGO as a low-cost, low-side-effect photo-immunotherapy reagent should be promising in the treatment of metastatic cancer. However, such a combination has not been explored.

We synthesized an inorganic nanocomposite by self-assembly of FNPs and rGO though electrostatic interaction and modification of PEG-NH_2, using a similar process proposed by Fu, et al., [34] but with a much more simplified procedure. The benefit of the excellent photothermal conversion ability of rGO and FNPs/rGO-PEG is to generate heat to kill the tumor cells by NIR laser irradiation. Subsequently, ICD elicited by PTT can release the tumor-associated antigens that can be captured and processed by antigen-presenting cells to induce a tumor-specific immune response. We characterized the FNPs/rGO-PEG and investigated its curative and immunological effects in treating metastatic tumors in mice. Specifically, we investigated the ICD with increased liberation of danger-associated molecular patterns (DAMPs) induced by FNPs/rGO-PEG based PTT. We also determined the immediate and long-term effects of FNPs/rGO-PEG based PTT in treating a metastatic breast tumor model in mice. We further studied the distribution and metabolism of FNPs/rGO-PEG in animals through MRI. Our results indicate that FNPs/rGO-PEG based PTT could be an effective approach for cancer treatment. Particularly due to the magnetic properties of FNPs/rGO-PEG, our study may also lead to an MRI-guided cancer therapy in the future.

Results and discussion

Synthesis and Characterization of FNPs/rGO-PEG

FNPs/rGO-PEG nanocomposites were obtained with a stepwise method (Fig. 2a). Oleate-capped Fe_3O_4 nanoparticle (FNPs) was prepared via high temperature decomposition. The average diameter of FNPs was 29 ± 4 nm with a relatively uniform size (Fig. 2b). To obtain hydrophilic FNPs, the oleate ligands were removed by ultrasonic oleate-capped FNPs in ethanol. Then, FNPs/rGO-PEG nanocomposites were achieved by conjugating hydrophilic FNPs with reduced-graphene oxide (rGO) through electrostatic adsorption, and also modified with PEG-NH_2. A TEM image (Fig. 2c) shows that the hydrophilic FNPs were successfully encapsulated in rGO-PEG, where the darker regions correspond to hydrophilic FNPs and the brighter regions correspond to rGO shells. The HRTEM, zeta potential, TGA were further confirmed the coupling of rGO-PEG and FNPs (Supplementary Fig. S1, S2, S3 and S4). The UV-Vis absorption spectra of FNPs/rGO-PEG showed that FNPs/rGO-PEG contained the characteristic absorption spectrum of FNPs and the broad-band absorption spectrum of rGO-PEG (Fig. 2d). The loading rate of rGO was calculated from the UV-Vis absorption spectra, 18.8 μg of rGO was loaded on 312.5 μg of FNPs.

Author Manuscript Author Manuscript Author Manuscript Author Manuscript

We also studied the photothermal properties of FNPs/rGO-PEG. The FNPs/rGO-PEG solution exhibited a rise in temperature from 20°C to nearly 60°C under an 805-nm laser irradiation within 6 min, whereas there was no significant temperature change in the solutions of PBS and FNPs, indicating an excellent photothermal conversion efficiency of FNPs/rGO-PEG (Fig. 2e). Infrared thermal images were also acquired to verify the FNPs/rGO-PEG + laser induced temperature increase (Fig. 2f). The magnetic relaxation of FNPs/rGO-PEG was determined (Fig. 2g). The T_2-weighted MR images of FNPs/rGO-PEG solutions with various Fe^{3+} concentrations showed a good dependence on the concentration gradient, indicating that the contrast was was effectively enhanced by FNPs/rGO-PEG. The *r2* value of FNPs/rGO-PEG measured at 7.1 Tesla is 116 (mM^{-1} s^{-1}), indicating FNPs/rGO-PEG is an excellent T_2 contrast agent.

In vitro photothermal therapy and immunogenic cell death of 4T1 tumor cells

We investigated the antitumor effect of FNPs/rGO-PEG *in vitro* by measuring the viability of 4T1 cells treated with FNPs, rGO-PEG, or FNPs/rGO-PEG under an 805-nm laser irradiation (5 min, 1 W/cm^2). The viabilities of 4T1 cells treated with FNPs/rGO-PEG + laser was reduced to 20% in 250 μg/mL FNPs/rGO-PEG solution, significantly lower than that treated with FNPs only, indicating that FNPs/rGO-PEG + laser exhibited a relatively high phototoxicity against to 4T1 cells (Fig. 3a). In contrast, no obvious cell death was observed at an FNPs/rGO-PEG dose of 250 μg/mL without light irradiation, indicating that the nanoparticles have good biocompatibility. The 4T1 tumor cell killing effect of FNPs/rGO-PEG was further verified via cell fluorescence images (Supplementary Fig. S7). We analysed HMGB1 release by enzyme-linked immunosorbent assay (ELISA). Compared with PBS + laser, FNPs + laser, and rGO-PEG + laser treatment, the FNPs/rGO-PEG + laser enhanced the HMGB1 release from 4T1 cells (Fig. 3b). The calreticulin (CRT) exposure of treated 4T1 tumor cells was evaluated. 4T1 tumor cells treated with FNPs/rGO-PEG + laser showed significant cell-surface CRT exposure (red), suggesting that FNPs/rGO-PEG + laser strongly induced CRT exposure on 4T1 tumor cells (Fig. 3c). These results demonstrate that FNPs/rGO-PEG based PTT could kill 4T1 tumor cells while enhancing the release of DAMPs.

Efficacy of photothermal therapy (PTT) against 4T1 tumors

The effects of FNPs/rGO-PEG based PTT was evaluated using a highly tumorigenic, poorly immunogenic 4T1 tumor model in mice. BALB/c mice were subcutaneously injected with 5 × 10^5 4T1 cells into the right breast pad. After the tumor reached a size of approximately 100 mm^3, the mice were divided into four treatment groups: PBS + laser, FNPs + laser, rGO-PEG + laser and FNPs/rGO-PEG + laser. After a one-hour post intratumoral injection of PBS, FNPs, rGO-PEG or FNPs/rGO-PEG solutions, the animal tumors were irradiated with an 805-nm laser for 10 min. Thermal imaging data showed that the surface temperature of tumors treated via FNPs/rGO-PEG + laser increased to 59°C and remained stable afterwards, in comparison to 42°C and 47°C when using PBS + laser or FNPs + laser (Fig. 4a and 4b). The photothermal effect was further verified via images of harvested tumor sections one day after treatment. Hematoxylin and eosin (H&E) staining (Fig. 4c) showed severe impairment of tumor structure in the rGO-PEG+ laser and FNPs/rGO-PEG+ laser groups confirming the *in vivo* photothermal effect of rGO-PEG and FNPs/rGO-PEG.

Author Manuscript Author Manuscript Author Manuscript Author Manuscript

The antitumor effect of FNPs/rGO-PEG + laser was additionally evaluated by monitoring tumor growth in response to treatment. The tumor growth in mice that received FNPs + laser showed no significant difference compared to mice receiving PBS + laser (Fig. 4d). In contrast, FNPs/rGO-PEG + laser completely regressed the tumors (Fig. 4d), and the regressed tumors did not grow back after initial irradiation. Besides, the mice body weight and tissue sections showed no significant change during treatments (Fig. 4e, Supplementary Fig. S8), indicating the safety of FNPs/rGO-PEG based PTT. The therapeutic efficacy of FNPs/rGO-PEG + laser also translated into improved animal survival of 16.67% (Fig. 4f). Although, both rGO + laser and FNPs/rGO-PEG + laser had the identical effect on treated primary tumors, only FNPs/rGO-PEG + laser yielded long-term survival (Fig. 4f). The median survival time of FNPs/rGO-PEG + laser group (44 days) is also longer than rGO-PEG + laser group (32 days). The data demonstrate that FNPs/rGO-PEG + laser is more effective in inhibiting tumor metastasis compared with rGO-PEG. The primary reason is that the FNPs in FNPs/rGO-PEG nanocomposite could inhibit the generation of M2 by changing the tumor microenvironment.

Antitumor immune responses induced by FNPs/rGO-PEG + PTT

Tumor-specific immune responses induced by FNPs/rGO-PEG based PTT were studied using a bilateral tumor model (Supplementary Fig. S9). The tumor on the right flank was treated while the tumor on the left flank was observed. First, the effects of FNPs/rGO-PEG based PTT on DCs were investigated by assessing the frequency of matured DCs ($CD11c^+CD86^+$) in lymph nodes of tumor-bearing mice 3 days post treatment. Combining FNPs/rGO-PEG with laser irradiation significantly promoted up to 30.2% of DCs maturation (Fig. 5a). The increase of infiltration was also demonstrated by the $CD11c^+$ expression level in treated tumors (Supplementary Fig. S10). It is apparent that the treatment by FNPs/rGO-PEG + laser induced the highest level of DCs infiltration and maturation. The antitumor immunity evoked by FNPs/rGO-PEG + laser was also studied by measuring the serum concentration of cytokines via enzyme-linked immunosorbent assays (ELISA). The serum levels of IL-12p70 (Fig. 5b) and IL-6 (Fig. 5c) in the FNPs/rGO-PEG + laser group were 4.84-fold and 5.27-fold higher than the control group, respectively, examined 3 days post treatment (Fig. 5b and 5c).

Furthermore, T cell activation was investigated after FNPs/rGO-PEG based PTT. As shown in Fig. 6a, flow cytometry analysis of splenocytes showed that FNPs + laser failed to promote $CD8^+$ activation. In contrast, mice treated with rGO PEG + laser andFNPs/rGO-PEG + laser had an increase in $CD8^+$ T cells activation of ~4.27% and ~4.97%, respectively. The increase of activation level of CD8+ by FNPs/rGO-PEG + laser was demonstrated by the $CD8^+$ expression in secondary tumors (Fig. 6e). In addition, higher level of expression of $CD8^+IFN\text{-}\gamma^+$ T cells was found in the FNPs/rGO-PEG + laser treatment group compared to other treatment groups. As compared with rGO-PEG + laser group, the T cell activation by FNPs/rGO-PEG based PTT was obviously higher, suggesting that FNPs/rGO-PEG based PTT is favorable for eliciting systemic T-cell activation. It is reported that FNPs could disassemble H_2O_2 into highly toxic hydroxyl radicals (•OH) which can change the acidic tumor microenvironment and induce a pro-inflammatory immune response with M1 macrophage polarization.[30–33] rGO-PEG has excellent photothermal properties, and it is

Author Manuscript Author Manuscript Author Manuscript Author Manuscript

also capable of eliciting strong immunological responses (such as M1 macrophage polarization).[29, 34–36] Combining with rGO-PEG with FNPs, FNPs/rGO-PEG nanocomposite-based phototherapy is favorable for triggering an antitumor immune response.

In vivo MR imaging

As shown in Fig. 7 and Supplementary Fig. S11, *in vivo* MR images of a tumor-bearing BALB/c mouse were acquired before and after intravenous injection of FNPs/rGO-PEG at different time frames to determine the distribution of FNPs/rGO-PEG. Strong T2 MR signals appeared in the tumor after injection of FNPs/rGO-PEG, and gradually increased over time within 3 h (Fig. 7). After 24 h, the T_2 MR signals were gradually reduced (Fig. 7). Our results indicated that FNPs/rGO-PEG could accumulate in the tumor within an hour (Supplementary Fig. S12). Moreover, imaging data of different tissues (Supplementary Fig. S12) showed that FNPs/rGO-PEG appeared to accumulate in the kidneys in 30 min post injection, as shown in Supplementary Fig. S12b with a time-dependent T2 signal. Due to the excellent magnetic properties of iron ions, FNPs/rGO-PEG may lead to an MRI-imaging guided photothermal-immunotherapy for metastatic cancers.

Experimental

Materials

Reduced graphene oxide (rGO), Iron (III) acetylacetonate, N-(3-Dimethylaminopropyl)-N'-ethylcarbodiimide hydrochloride (EDC), N-hydroxysuccinimide (NHS), dimethyl sulfoxide (DMSO), oleic acid (OA), and benzyle ether were purchased from Sigma- Aldrich (USA). RPMI 1640, Trypsin-EDTA, and PBS (pH 7.4) were bought from Gibco Life Technologies (USA). PEG_{2K}-NH_2 was purchased from Avanti Polar Lipids (USA).

Cell lines and animals

The 4T1 cell line was obtained from the American Type Culture Collection (ATCC). Female BALB/c mice (4 - 6 weeks) were purchased from Charles River (Wilmington, MA, USA). Mice were housed in animal facility of the Department of Comparative Medicine at the University of Oklahoma Health Sciences Center (OUHSC, Oklahoma, USA). All experiments were performed in accordance with NIH publication and guidelines for the care and use of Laboratory Animals approved by the OHUSC Institutional Animal Care and Use Committee.

Synthesis of FNPs

Oleate-capped FNPs were first prepared by mixing iron (III) acetylacetonate (2 mmol), oleic acid (0.5 mL), and benzyle ether (20 mL) in a 100 mL round-bottom, three-necked flask, followed by heating at 160 °C for 30 min under N_2 at the appropriate flow rate. Then, the solution was heated to 280°C for 30 min. After cooling to room temperature, the resulting oleate-capped FNPs were collected via ethanol addition, centrifuged at 6,000 rpm for 10 min, and washed with ethanol three times. Then, the oleate-capped FNPs were re-dispersed in 20 mL of ethanol and sonicated for 30 min to remove the oleic acid on the surface of

Author Manuscript Author Manuscript Author Manuscript Author Manuscript

FNPs. After washing with an ethanol/ deionized water solution (v / v: 50 / 50) three times, the final FNPs were stored in deionized water for further use.

Synthesis of FNPs/rGO

FNPs (10 mg) and rGO (2 mg) were mixed in 5 mL H_2O and sonicated in a water bath for 10 min. Then the solution was stirred at room temperature for 12 h. The resulting nanocomposites were collected via centrifugation at 11000 rpm for 10 min, washed 3 times with deionized water, and re-dispersed in 10 mL of deionized water for further use.

Synthesis of FNPs/rGO-PEG

FNPs/rGO were also conjugated with PEG2000-NH_2 following a well-established EDC/NHS protocol. FNPs/rGO (20 mg) dissolved in 5 mL DMSO were activated with 20 mM EDC and 50 mM NHS for 4 hours at room temperature. Then, the activated FNPs/rGO nanocomposites were incubated with 50 mg PEG_{2K}-NH_2 in 10 mL PBS (pH 7.4). After overnight shaking at room temperature, FNPs/rGO-PEG were collected via centrifugation at 13800 rpm for 10 min, washed 3 times with deionized water, and re-dispersed in 10 mL of deionized water for further use. Before applying rGO-PEG or FNPs/rGO-PEG to cells or to the mice, the nanomaterial was washed with sterile ultrapure water repeatedly, and further sterilized by UV light. All operations were performed in a clean bench to ensure sterility of the experiment.

Characterization of Nanoparticles

The morphology of FNPs, rGO-PEG and FNPs/rGO-PEG was characterized by transmission electron microscopy (TEM) and using a JEOL-2010 TEM (JEOL, Japan). The UV-Vis absorption spectra of FNPs, rGO-PEG and FNPs/rGO-PEG nanocomposites were measured by UV-Vis absorption spectrophotometer (Cary 50 Bio, USA).

In vitro photothermal therapy of FNPs/rGO-PEG

For cell viability, 4T1 cells were seeded into 96-well plates at a density of 5×10^3 cells per well and cultured for 12 h. Cells were treated with various concentrations of PBS, FNPs, rGO-PEG, and FNPs/rGO-PEG. After 4 h of incubation, the cells were irradiated with an 805-nm semiconductor laser (AngioDynamics, Inc.,USA) for 5 min (1 W/cm^2) or separately kept in dark. Cells were further incubated for 24 h and cell viability was determined by CCK-8 assay according to the manufacturer's protocol. For fluorescent imaging, 4T1 cells were stained with calcein AM and PI 24 h after irradiation with an 805-nm laser and then imaged using a fluorescence microscope (Olympus, Japan).

DAMPs expression analysis

The surface exposure of CRT was assessed by immunofluorescence imaging. 4T1 tumor cells were seeded into 8-well chambered slides at a density of 8×10^3 cells per well and cultured for 12 h. Cells were incubated with PBS, FNPs, rGO-PEG, and FNPs/rGO-PEG nanocomposites. After 4 h of incubation, the cells were irradiated with a 1 W/cm^2 of 805-nm laser for 5 min. Cells treated with FNPs/rGO-PEG without laser irradiation were used as a dark control. After an additional 24 h of incubation, the cells were incubated with anti-

Author Manuscript Author Manuscript Author Manuscript Author Manuscript

calreticulin antibody for 2 h at 4 °C. Subsequently, the cells were washed twice with PBS and incubated with Alexa Fluor 647-conjugated secondary antibody (Life technologies, USA) for 1 h. After staining with DAPI, the cells were observed under a fluorescence microscope. The extracellularly released HMGB1 was examined using the HMGB1 ELISA Kit. Briefly, 4T1 cells were seeded in 24-well plates (5×10^4 cells/well) and cultured for 12 h. Cells were incubated with PBS, FNPs, rGO-PEG, and FNPs/rGO-PEG nanocomposites. After 2 h of incubation, the cells were irradiated with a 1 W/cm^2 of 805-nm laser for 5 min. Cells treated with FNPs/rGO-PEG without laser irradiation were used as a dark control. After 12 h of incubation with additional ACC, the cell supernatant was collected. The release of HMGB1 in the cell supernatant was detected by the HMGB1 ELISA Kit according to the manufacturer's protocols.

In vivo photothermal therapy

BALB/c mice were subcutaneously injected with 5×10^5 4T1 cells into the right breast pad. When the tumors reached 100-150 cm^3, the mice were randomly divided into four groups (n = 6) and PBS, FNPs, rGO-PEG, FNPs/rGO-PEG nanocomposite was intratumorally injected (0.1 mg respectively). Two hours after injection, the mice were anaesthetized with 2% (v / v) isoflurane and tumors were irradiated with an 805-nm laser for 10 min at 1 W/cm^2. The light was delivered to the tumor using a fiber optic delivery system. The power density at the treatment area, which encompassed the tumor and 0.5 cm of the surrounding skin, was 1 W/cm^2 for treatment duration of 10 min. Besides, the rest part was covered with foil to avoid the thermal damage to surrounding healthy tissue. During laser irradiation, mice were restrained in a specially designed holder. Local tumors temperature was measured during laser irradiation of an 805-nm laser using an infrared thermal camera (FLIR, USA).

Anticancer efficacy in the 4T1 orthotopic mouse breast cancer model

The laser treatment procedures follow section above. The sizes of the tumors were measured every 2 days using a digital caliper and the volume was estimated by ellipsoidal calculation as $V = (\text{width})^2 \times \text{length} \times \pi/6$. When the tumors reached the maximum allowable size (2.0 cm in any dimension), the mice were euthanized or ulcerated.

Flow cytometric studies

The spleens were harvested and grinded using the rubber tip of the syringe, after which the red blood cells were removed by ACK lysis buffer. The cells were filtered through nylon mesh filters and washed with PBS. The single-cell suspensions were incubated with anti-CD16/32 (clone 93; eBioscience) to reduce non-specific binding to Fc receptors (FcRs). For analysis of the activated DCs, cells were stained with anti-mouse CD11c-APC and anti-mouse CD86-FITC antibodies. For analysis of active T cells in the spleens, cells were stained with Live/Dead-BV510, anti-mouse CD3-AF700, anti-mouse CD4-APC, and anti-mouse CD8a-FITC. The Stratedigm S1200Ex flow cytometer (Stratedigm) was used for flow cytometry, and data analysis was performed using FlowJo software.

Author Manuscript Author Manuscript Author Manuscript Author Manuscript

Detection of cytokines

Serum samples were isolated from mice after expansion of different types of treatment and analysis. According to the Vendors' protocols, both IL-12 (Dakewe biotech) and IL-6 (Dakewe biotech) were tested using an ELISA kits.

Immunofluorescence assay

Tumors were collected and 6 mm thick frozen tissue sections were prepared using a cryostat. The sections were air-dried for at least 1 h and then fixed in acetone for 10 min at room temperature. After blocking with 20% donkey serum, the sections were incubated with antibodies and washed twice with PBS, and observed under fluorescence microscopy (Olympus, Japan).

Small animal MRI

BALB/c mice were subcutaneously injected with 5×10^5 4T1 cells into the right breast pad. When the tumors reached 100 – 150 cm^3, all mice underwent magnetic resonance (MR) imaging under isoflurane anaesthesia. A 7.1 Tesla MR scanner (Bruker Biospin 7/30) was used in this experiment which parameters have a 40 mm Bruker Biospin quadrature radiofrequency volume coil (Bruker Biospin, Ettlingen, Germany) and a T_2*-weighted 2D fast gradient echo (FGRE) pulse sequence with a flip angle of 20°, a repetition time of 70 ms, multiple echo times of 1.5 – 12.6 ms (8 echoes with echo spacing of 1.6 ms), a matrix of 128×128 pixels, a field of view of 4.5×2.7 cm^{-2}, one excitation and a slice thickness of 0.6 mm. T_2* relaxation time maps were generated from multi-echo FGRE images by fitting the relaxation equation: $M(TE)^2 = M^20 \exp(-2TE / T_2*)$ to the image data using a custom research software (Cinetool,GE Global Research Center). T_2* relaxation times, which are proportional to local iron concentrations, were measured on T_2* relaxation time maps and compared between iron-co-injected and control implantation sites, using a t-test.

Statistical analysis

Data were analyzed using GraphPad Prism software and the values were expresses as mean ± S.E.M. Statistical analysis was performed using one-way ANOVA with Dunnett's multiple comparison test. P values <0.05 were considered statistically significant.

Conclusions

In this work, we developed a nanocomposite that could effectively eliminate primary tumors and induce antitumor immunity under irradiation from an 805-nm laser. This nanocomposite was synthesized by self-assembly of FNPs and rGO though electrostatic interaction, followed by modification with PEG-NH_2. Under laser irradiation, FNPs/rGO-PEG was able to improve the efficacy of PTT by increasing the temperature up to 60°C and killing 80% of tumor cells. Studies using similar nanoplatforms and laser irradiation have been conducted by Fu, et al. with promising therapeutic effects in treating animal tumors.[34] Our current study supported their results and, at the same time, further explored the immunological responses induced by the combination of nanoplatform and NIR laser irradiation. Our FNPs/rGO-PEG nanocomposites could be used to directly destroy tumor cells by PTT and to stimulate immune responses by triggering the maturation of DCs and the secretion of

Author Manuscript Author Manuscript Author Manuscript Author Manuscript

cytokines. In our animal experiments, when combined with NIR laser irradiation, nanocomposites could not only destroy the primary tumor, but also effectively improve the antitumor immune response. Our results showed that mice treated with FNPs/rGO-PEG based PTT had a significantly longer survival time. Furthermore, FNPs/rGO-PEG nanocomposites were able to be used for MRI-guided cancer photothermal-Immunotherapy due to their excellent magnetic properties. Therefore, this work has demonstrated the great potential of integrating FNPs/rGO-PEG based PTT with cancer immunotherapy to lead to an MRI-guided photothermal-immunotherapy for metastatic cancers, for the elimination of primary tumors, and the inhibition of distant tumors and to prevent tumor recurrence. This FNPs/rGO-PEG complex could be used for the development of various future photomedicine platforms.

Supplementary Material

Refer to Web version on PubMed Central for supplementary material.

Acknowledgements

This work was supported in part by the grants from the US National Institutes of Health (R21 EB015509, RS20132225-106, R01 CA205348), from the Oklahoma Center for Advancement of Science and Technology (HR16-085), from the China Postdoctoral Science Foundation (2018M633116) and the Natural Science Foundation of Fujian Province (2016J05060).

Notes and references

1. Rankin EB and Giaccia AJ, Science, 2016, 352, 175–180. [PubMed: 27124451]
2. Schroeder A, Heller DA, Winslow MM, Dahlman JE, Pratt GW, Langer R, Jacks T and Anderson DG, Nat. Rev. Cancer, 2011, 12, 39. [PubMed: 22193407]
3. O'Shaughnessy J, Osborne C, Pippen JE, Yoffe M, Patt D, Rocha C, Koo IC, Sherman BM and Bradley C, N. Engl. J. Med, 2011, 364, 205–214. [PubMed: 21208101]
4. Steeg PS, Nat. Med, 2006, 12, 895. [PubMed: 16892035]
5. Chen Z, Liu L, Liang R, Luo Z, He H, Wu Z, Tian H, Zheng M, Ma Y and Cai L, ACS Nano, 2018, 12, 8633–8645. [PubMed: 30005164]
6. Xu J, Xu L, Wang C, Yang R, Zhuang Q, Han X, Dong Z, Zhu W, Peng R and Liu Z, ACS Nano, 2017, 11, 4463–4474. [PubMed: 28362496]
7. Dudley ME, Yang JC, Sherry R, Hughes MS, Royal R, Kammula U, Robbins PF, Huang J, Citrin DE, Leitman SF, Wunderlich J, Restifo NP, Thomasian A, Downey SG, Smith FO, Klapper J, Morton K, Laurencot C, White DE and Rosenberg SA, J. Clin. Oncol, 2008, 26, 5233–5239. [PubMed: 18809613]
8. Ledford H, Nature, 2013, 497, 544. [PubMed: 23719439]
9. Vanneman M and Dranoff G, Nat. Rev. Cancer, 2012, 12, 237. [PubMed: 22437869]
10. Zhao Y, Luo Z, Li M, Qu Q, Ma X, Yu S-H and Zhao Y, Angew. Chem. Int. Edit, 2015, 54, 919–922.
11. Wang C-Q, Gong M-Q, Wu J-L, Zhuo R-X and Cheng S-X, RSC Adv, 2014, 4, 38623–38629.
12. Shi H, Li L, Zhang L, Wang T, Wang C, Zhu D and Su Z, CrystEngComm, 2015, 17, 4768–4773.
13. Chen S, Zhao D, Li F, Zhuo R-X and Cheng S-X, RSC Adv, 2012, 2, 1820–1826.
14. Locke A, Pra AD, Supiot S, Warde P and Bristow RG, Nat. Rev. Urol, 2015, 12, 193. [PubMed: 25800395]
15. Zhong X, Yang K, Dong Z, Yi X, Wang Y, Ge C, Zhao Y and Liu Z, Adv. Funct. Mater, 2015, 25, 7327–7336.

Author Manuscript Author Manuscript Author Manuscript Author Manuscript

16. Akhter S, Ahmad MZ, Ahmad FJ, Storm G and Kok RJ, Expert Opin. Drug Del, 2012, 9, 1225–1243.
17. Kong F, Zhang H, Qu X, Zhang X, Chen D, Ding R, Mäkilä E, Salonen J, Santos HA and Hai M, Adv. Mater, 2016, 28, 10195–10203. [PubMed: 27689681]
18. Yang G, Xu L, Chao Y, Xu J, Sun X, Wu Y, Peng R and Liu Z, Nat. Commun, 2017, 8, 902. [PubMed: 29026068]
19. Pai C-L, Chen Y-C, Hsu C-Y, Su H-L and Lai P-S, J. Biomed. Nanotechnol, 2016, 12, 619–629. [PubMed: 27301189]
20. Wang C, Xu L, Liang C, Xiang J, Peng R and Liu Z, Adv. Mater, 2014, 26, 8154–8162. [PubMed: 25331930]
21. Chen Q, Xu L, Liang C, Wang C, Peng R and Liu Z, Nat. Commun, 2016, 7, 13193. [PubMed: 27767031]
22. Cheng L, Wang C, Feng L, Yang K and Liu Z, Chem. Rev, 2014, 114, 10869–10939. [PubMed: 25260098]
23. Sherlock SP, Tabakman SM, Xie L and Dai H, ACS Nano, 2011, 5, 1505–1512. [PubMed: 21284398]
24. Tao Y, Ju E, Ren J and Qu X, Biomaterials, 2014, 35, 9963–9971. [PubMed: 25224368]
25. Guo L, Yan DD, Yang D, Li Y, Wang X, Zalewski O, Yan B and Lu W, ACS Nano, 2014, 8, 5670–5681. [PubMed: 24801008]
26. Kostarelos K, Bianco A and Prato M, Nat. Nanotechnol, 2009, 4, 627. [PubMed: 19809452]
27. Li X, Naylor MF, Le H, Nordquist RE, Teague TK, Howard CA, Murray C and Chen WR, Cancer Biol. Ther, 2010, 10, 1081–1087. [PubMed: 20890121]
28. Zhou F, Wu S, Song S, Chen WR, Resasco DE and Xing D, Biomaterials, 2012, 33, 3235–3242. [PubMed: 22296829]
29. Luo N, Weber JK, Wang S, Luan B, Yue H, Xi X, Du J, Yang Z, Wei W, Zhou R and Ma G, Nat. Commun, 2017, 8, 14537. [PubMed: 28233871]
30. Zanganeh S, Hutter G, Spitler R, Lenkov O, Mahmoudi M, Shaw A, Pajarinen JS, Nejadnik H, Goodman S, Moseley M, Coussens LM and Daldrup-Link HE, Nat. Nanotechnol, 2016, 11, 986–994. [PubMed: 27668795]
31. Feng L, Xie R, Wang C, Gai S, He F, Yang D, Yang P and Lin J, ACS Nano, 2018, 12, 11000–11012. [PubMed: 30339353]
32. Shen Z, Liu T, Li Y, Lau J, Yang Z, Fan W, Zhou Z, Shi C, Ke C, Bregadze VI, Mandal SK, Liu Y, Li Z, Xue T, Zhu G, Munasinghe J, Niu G, Wu A and Chen X, ACS Nano, 2018, 12, 11355–11365. [PubMed: 30375848]
33. Tao Y, Ju E, Ren J and Qu X, Biomaterials, 2014, 35, 9963–9971. [PubMed: 25224368]
34. Fu G, Zhu L, Yang K, Zhuang R, Xie J and Zhang F, ACS Appl. Mater, 2016, 8, 5137–5147.
35. Feito MJ, Diez-Orejas R, Cicuéndez M, Casarrubios L, Rojo JM and Portolés MT, Colloid. Surface. B, 2019, 176, 96–105.
36. Miao X, Leng X and Zhang Q, Int. J. Mol. Sci, 2017, 18, 336.

Author Manuscript Author Manuscript Author Manuscript Author Manuscript

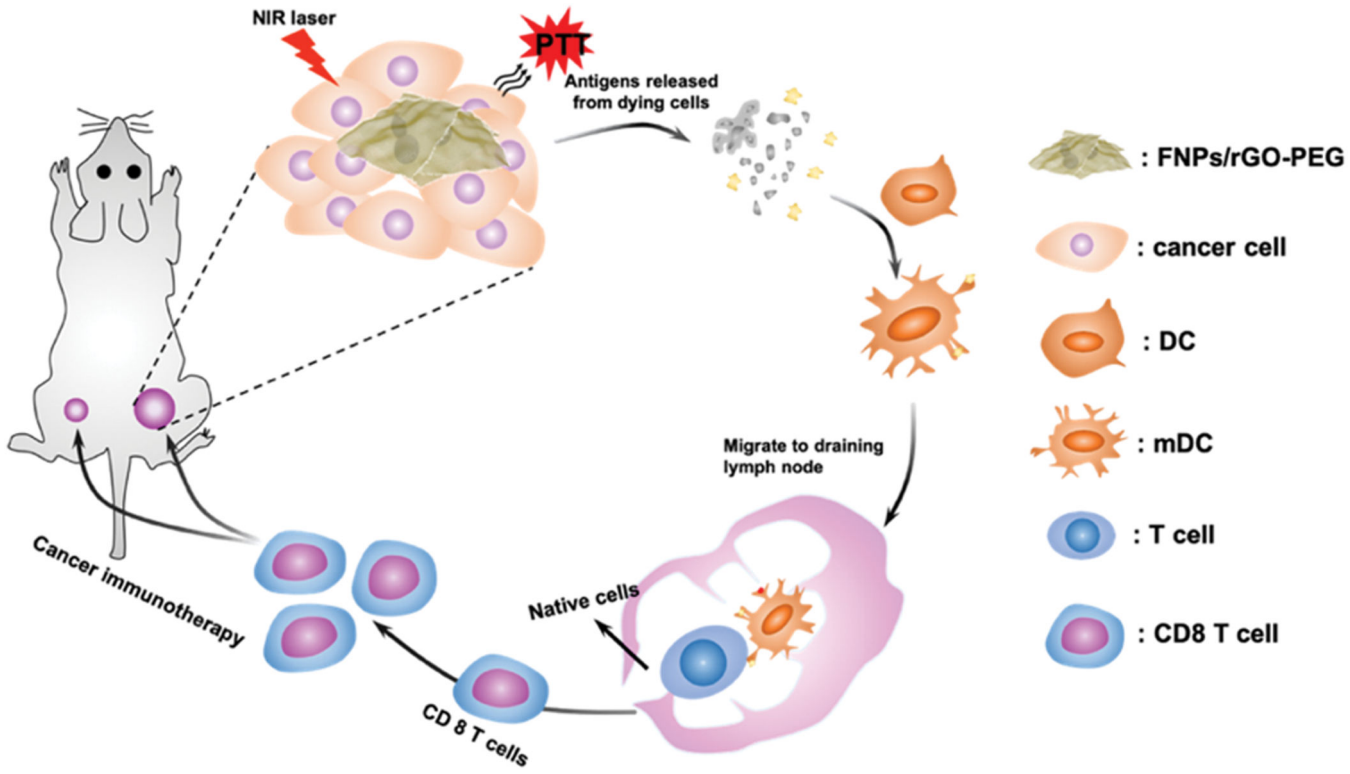

Fig. 1.

Schematic depiction of NIR-mediated photothermal-immunotherapy with FNPs/rGO-PEG nanocomposites for destruction of primary tumors and eliciting anti-metastatic effect. Under laser irradiation, FNPs/rGO-PEG nanocomposites could generate heat and trigger immunogenic cell death (ICD). Then, the released tumor-associated antigens could trigger maturation of dendritic cells (DCs). DCs could capture the antigens and migrate to tumor draining lymph node to present the antigens and activate T-cells. FNPs/rGO-PEG based PTT could effectively induce a systemic antitumor immunity to eliminate metastases and prevent tumor recurrence.

Author Manuscript Author Manuscript Author Manuscript Author Manuscript

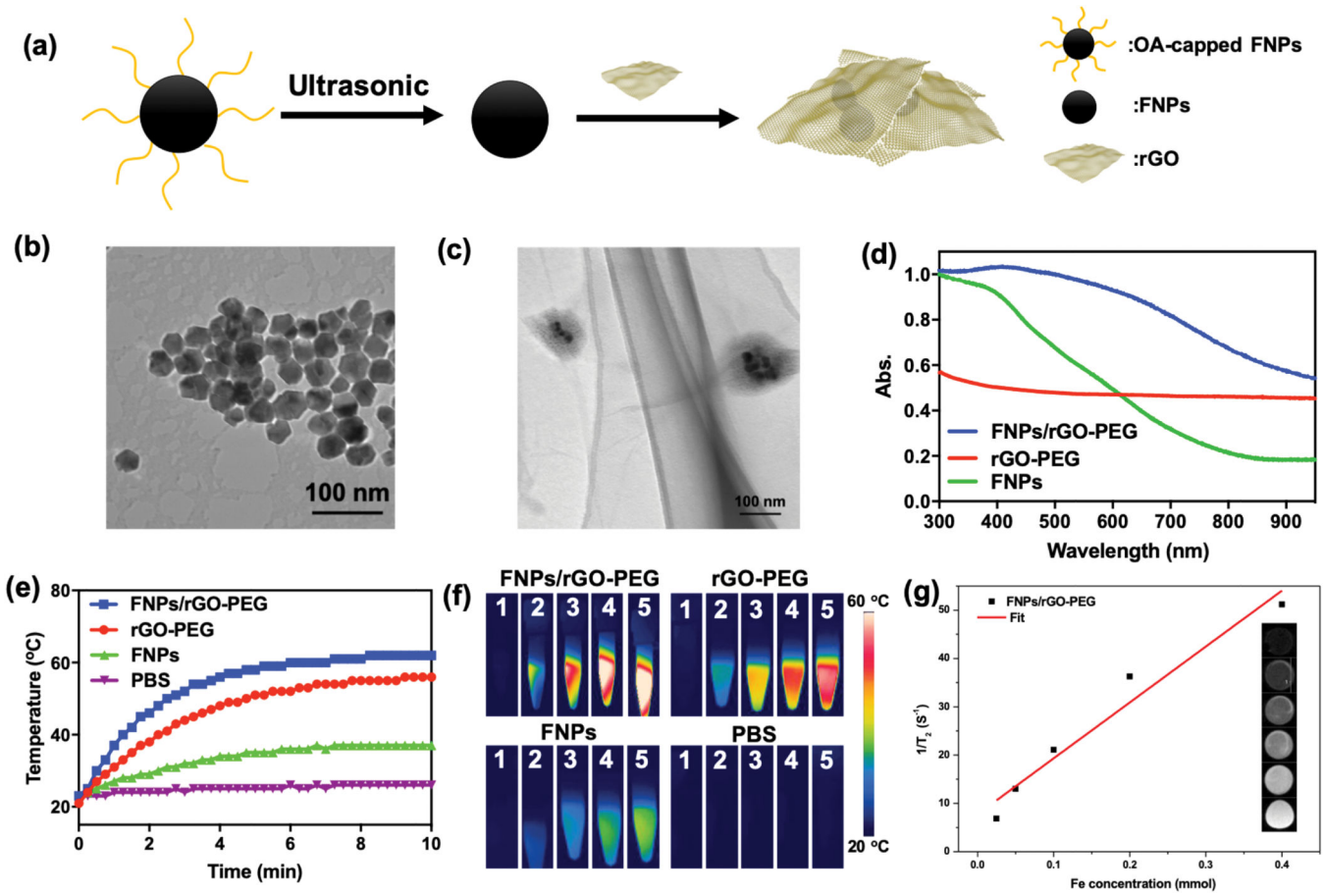

Fig. 2.

Characterization of FNPs, rGO-PEG and FNPs/rGO-PEG. (a) Schematic of fabrication process of FNPs/rGO-PEG. (b) Transmission electron microscopy (TEM) images of (b) FNPs and (c) FNPs/rGO-PEG. Scar bar = 100 nm. (d) UV–Vis absorption spectrum of FNPs (0.5 mg mL^{-1}), rGO-PEG (40 μg mL^{-1}) and FNPs/rGO-PEG (0.5 mg mL^{-1}). The broad-band absorption spectrum of FNPs/rGO-PEG around 800 nm indicates the conjugation of FNPs and rGO. (e) Photothermal effects of aqueous FNPs (0.5 mg mL^{-1}), rGO-PEG (40 μg mL^{-1}) and FNPs/rGO-PEG (0.5 mg mL^{-1}) under NIR laser irradiation (λ = 805 nm; 1.0 W/cm^2) for 10 min. (f) Infrared thermal images before (1) and during (2-5) NIR irradiation, at an interval of 1 minute. (FNPs: 0.5 mg mL^{-1}, rGO: 40 μg mL^{-1}, FNPs/rGO-PEG: 0.5 mg mL^{-1}) (g) The variation of $1/T_2$ with Fe concentration of FNPs/rGO-PEG measured by a 7.1-T magnetic resonance imager. The r_2 relativity was 116 (mM^{-1} s^{-1}) obtained from fitting the slope of each sample. The insets show the T_2-weighted images of FNPs/rGO-PEG at different Fe concentrations.

Author Manuscript Author Manuscript Author Manuscript Author Manuscript

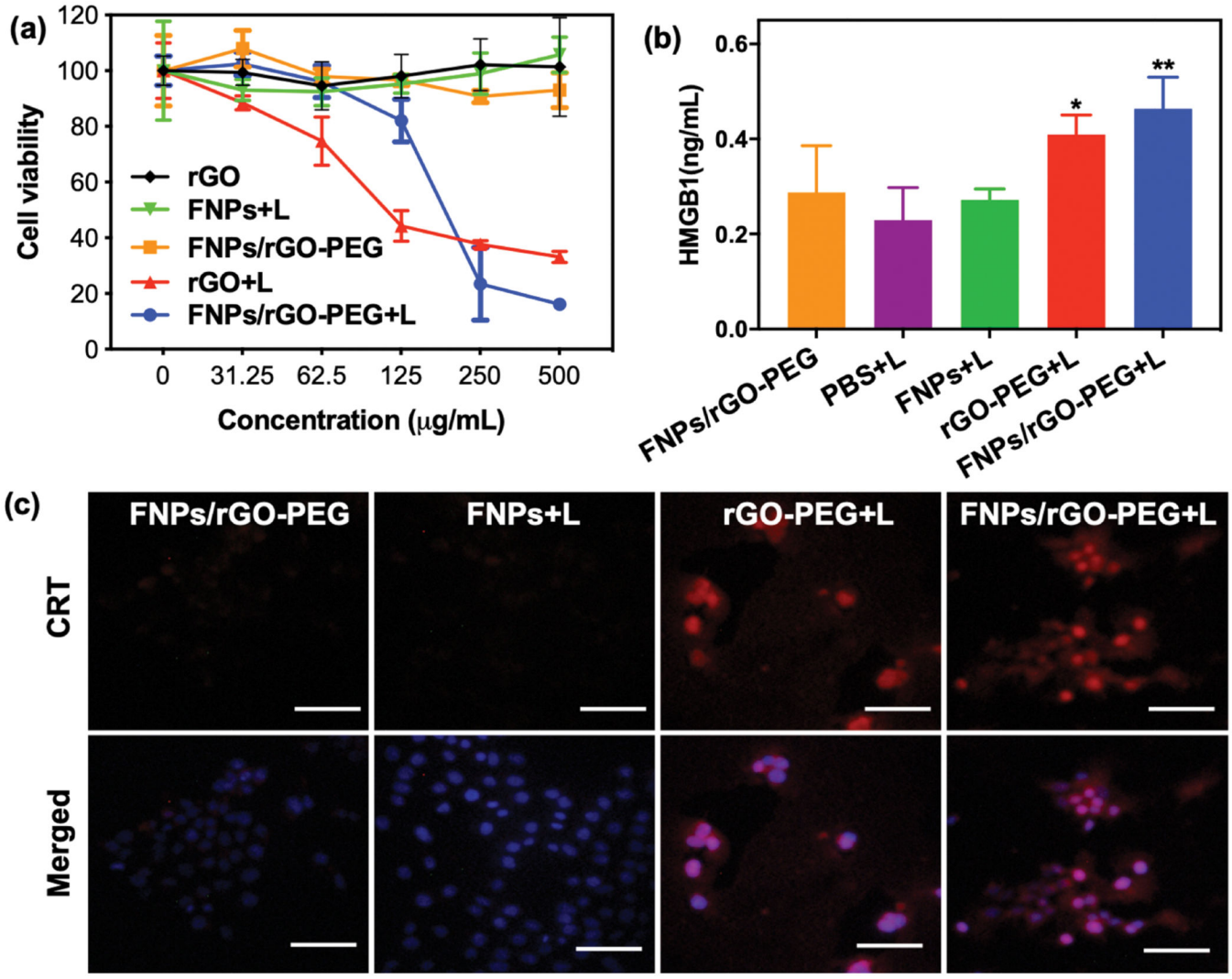

Fig. 3.

In vitro PTT and immunogenic cell death triggered by FNPs/rGO-PEG. (a) The viability of 4T1 cells incubated with FNPs, rGO-PEG or FNPs/rGO-PEG at different concentrations for 4 h and treated with laser irradiation (λ = 805 nm; 1.0 W/cm^2) for 5 min. CCK-8 assay was used 2 h after the treatment to determine the cell viability. (rGO: 0, 2.5, 5, 10, 20, 40 μg mL^{-1}; FNPs and FNPs/rGO-PEG: 0, 31.25, 62.5, 125, 250, 500 μg mL^{-1}) (b) Detection of extracellular HMGB1 after different treatments of 4T1 cells as in (a). Data are presented as the mean ± S.E.M. (*P < 0.05; **P < 0.01). (c) Fluorescence images of CRT exposed on the surface of 4T1 tumor cells after different treatments as in (a). Scale bar = 100 μm.

Author Manuscript Author Manuscript Author Manuscript Author Manuscript

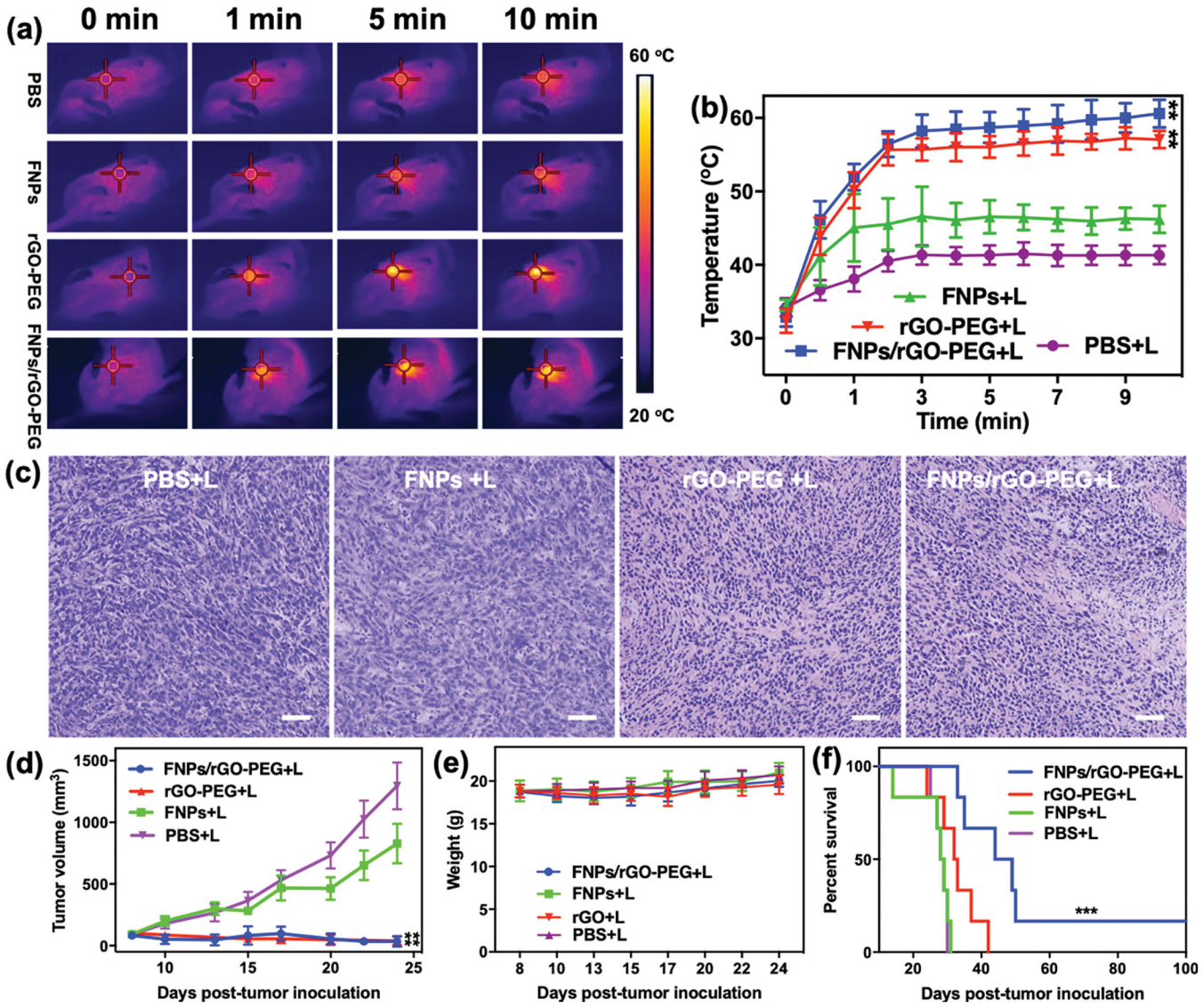

Fig. 4.

In vivo photothermal response and *in vivo* antitumor effect of phototherapy. (a) Infrared thermal images of 4T1 tumor-bearing mice at 0, 1, 5 and 10 min during NIR laser irradiation (805 nm, 1 W/cm^2). Red target circles indicate tumor location. (b) Temperature changes in the tumor area at different time points during the laser irradiation (n = 6). (c) Representative H&E-stained images of 4T1 tumors after different treatments as indicated. Scale bar = 100 μm. (d) Growth curves for tumors on 4T1 tumor-bearing mice treated with intratumoral injection (100 μL) of PBS, FNPs (10 mg/mL), rGO-PEG (2 mg/mL) and FNPs/rGO-PEG (10 mg/mL), followed by PTT for 10 min (λ = 805 nm; 1.0 W/cm^2) (n = 6). Treatments began when the primary tumors reached a size of 100–150 mm^3. (e) Body weights of mice in different groups during the course of treatment (n = 6). (f) Survival rate of mice in different groups of mice bearing orthotopic 4T1 tumor (6 mice per group). Data are presented as the mean ± S.E.M. (**P < 0.01 vs PBS+L; ***P < 0.001 vs PBS+L)

Author Manuscript Author Manuscript Author Manuscript Author Manuscript

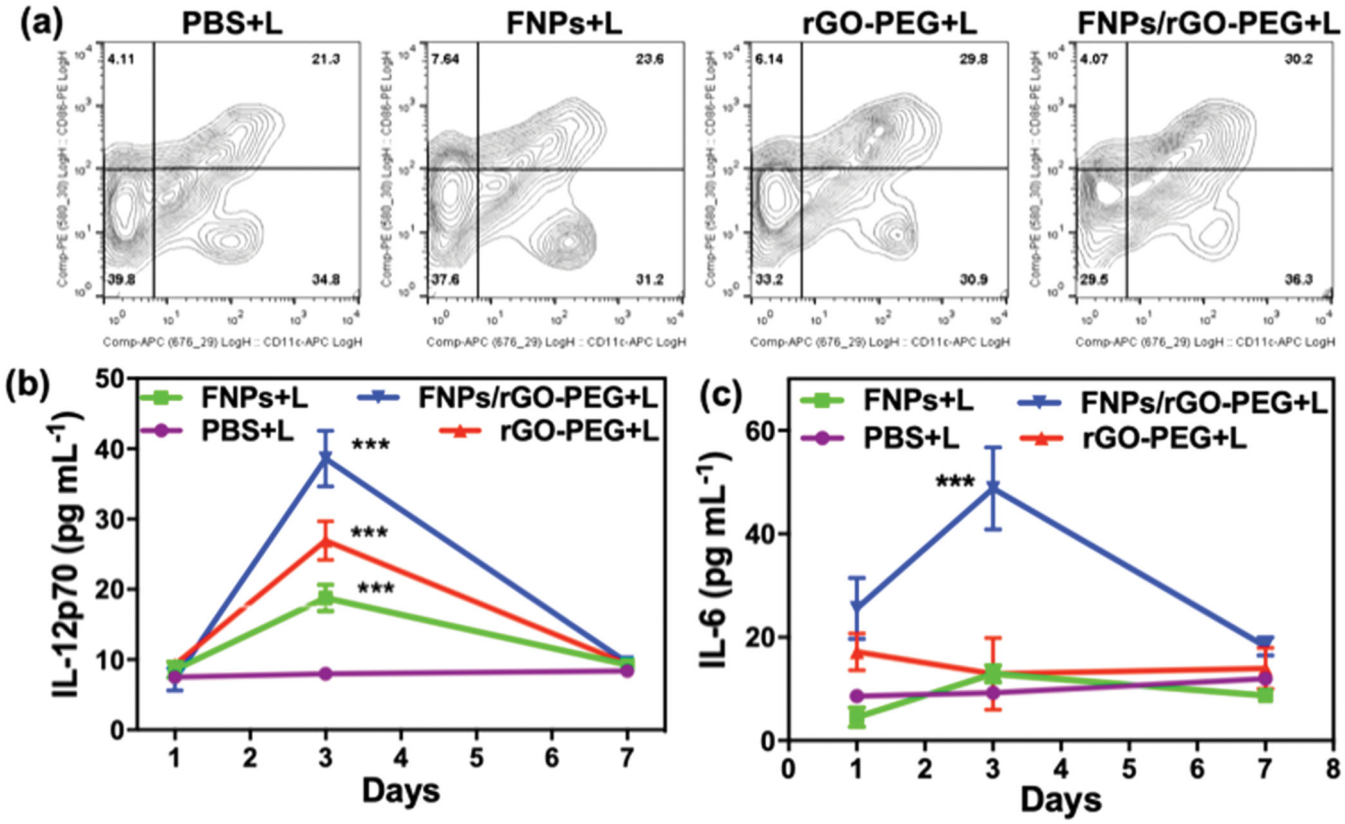

Fig. 5.

In vivo immune responses. (a) The frequency of mature DCs ($CD11c^{+}CD86^{+}$) in tumor draining lymph nodes of mice 3 days after different treatments. Serum concentrations of IL-12p70 (b) and IL-6 (c) examined at desired time points post treatment (n = 4). Data are presented as the mean ± S.E.M. (***P < 0.001 vs PBS+L).

Author Manuscript Author Manuscript Author Manuscript Author Manuscript

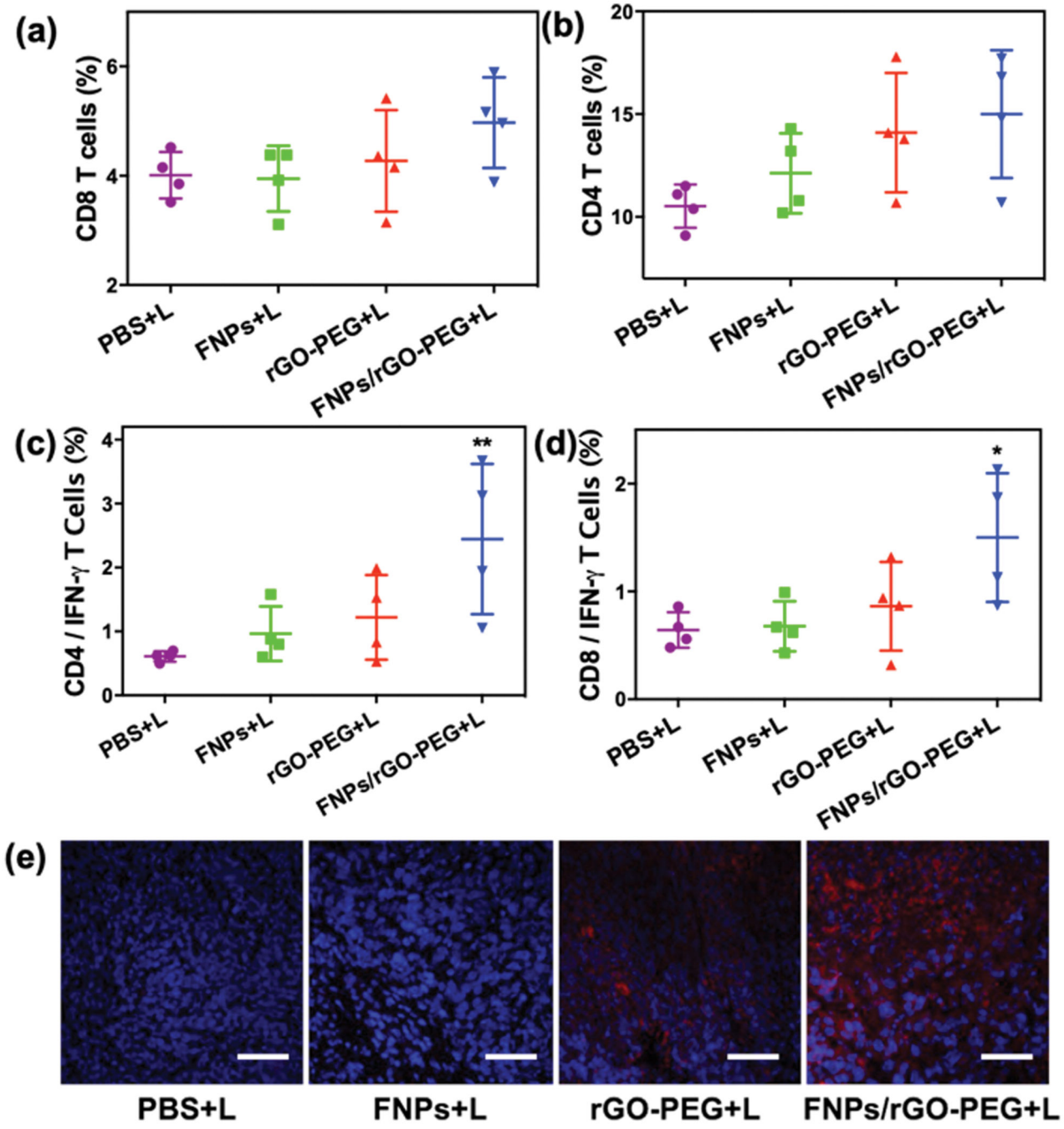

Fig. 6.

Induced tumor-specific immune responses. Flow cytometric analysis of the relative abundance of CD8 (a) and CD4 (b) T cells subpopulations in spleens of mice after different treatments of orthotopic 4T1 tumors (n = 4). Flow cytometric analysis of the IFN-γ secreting CD8 (d) and CD4 (c) T cells in the spleens of mice with different treatment (n = 4). (e) Immunofluorescence staining of CD8 T cells (red) in the untreated second tumor tissue. Scar bar = 200 μm. Data are presented as the mean ± S.E.M. (*P < 0.05 vs PBS+L; **P < 0.01 vs PBS+L).

Author Manuscript Author Manuscript Author Manuscript Author Manuscript

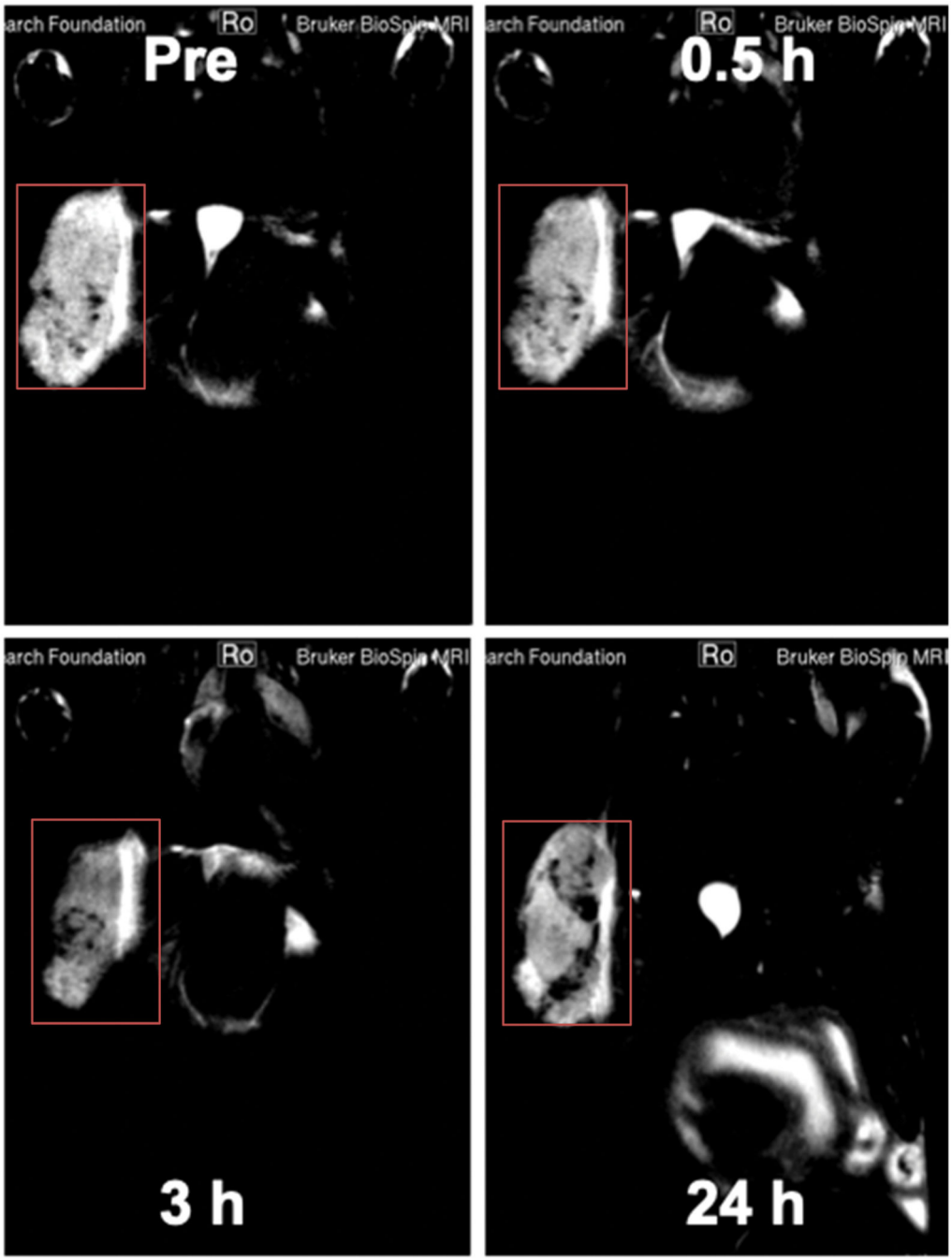

Fig. 7.

In vivo MR images of a tumor-bearing mouse before and after intravenous injection of FNPs/rGO-PEG at different time frames (0, 0.5 h, 3 h and 24 h). Red squares indicate tumor site.